PNAS

Supporting Information for

Activation of P53 pathway contributes to *Xenopus* hybrid inviability

Zhaoying Shi†, Guanghui Liu†, Hao Jiang†, Songyuan Shi, Xuan Zhang, Yi Deng,

Yonglong Chen*

Yonglong Chen

Email: chenyl@sustech.edu.cn

This PDF file includes:

Figures S1 to S8

Tables S1

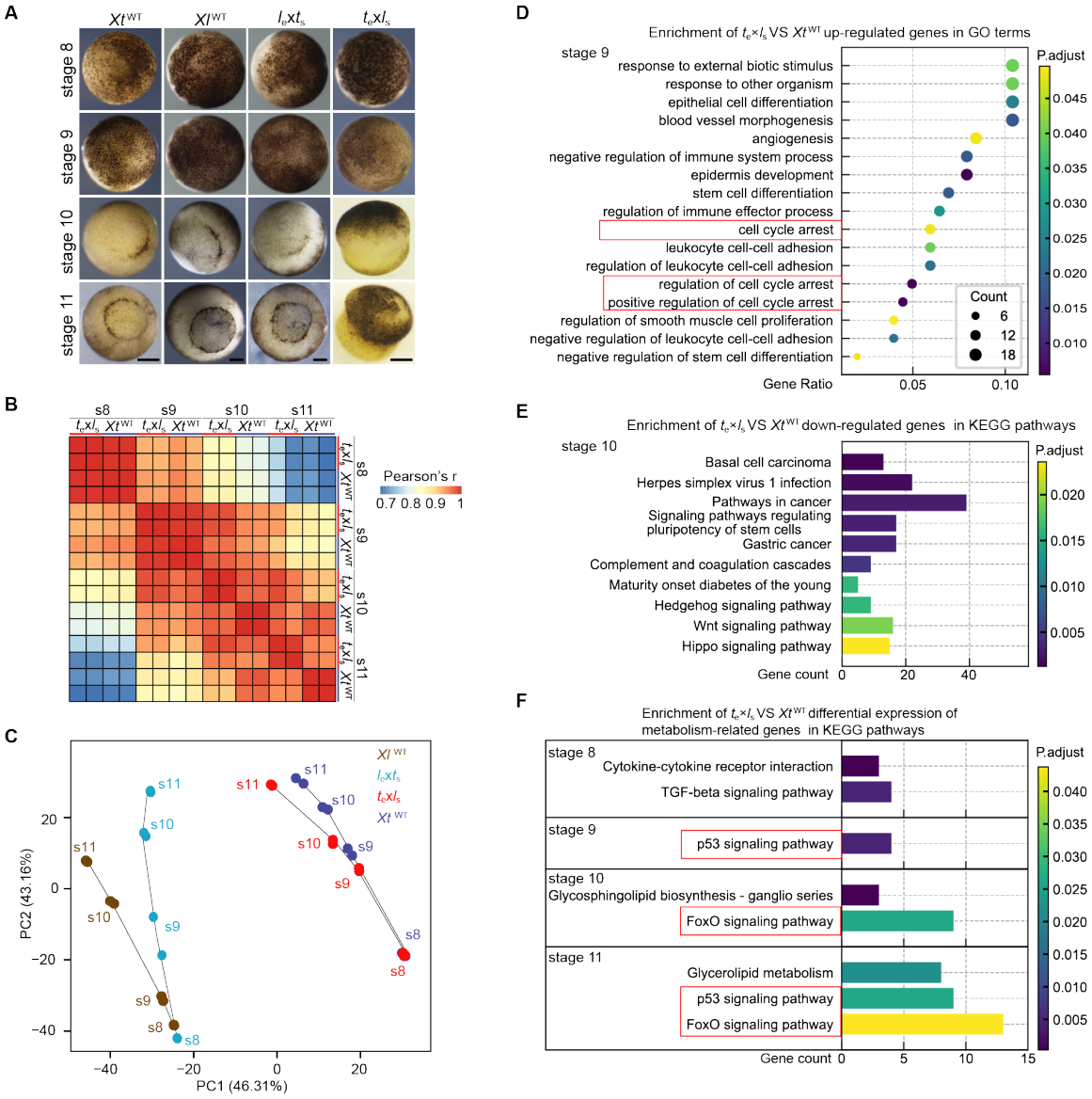

Figure S1. Phenotype characterization of $t_e \times l_s$ embryos using RNA-seq analysis. (A) Representative images of wild-type and hybrid embryos. Identical results were obtained with more than 6 times of independent cross-fertilization experiments. Scale bars, 200 μm. **(B)** Pearson's correlation of the RNA-seq profiles from stage 8 to stage 11. s, stage. **(C)** Principal component analysis (PCA) of transcriptomes showing strong maternal effects during early development. **(D)** Gene ontology (GO) terms enriched in up-regulated genes between $t_e \times l_s$ and Xt^{WT} at stage 9. The red boxes highlight genes enriched in cell cycle arrest. **(E)** KEGG pathway enrichment analysis for down-regulated genes between $t_e \times l_s$ and Xt^{WT} at stage 10. Wnt and Hedgehog signaling pathways were down-regulated. **(F)** KEGG pathway enrichment analysis for differentially expressed metabolism genes. Red boxes highlight enrichment of P53 and FoxO pathways during stages 9-11.

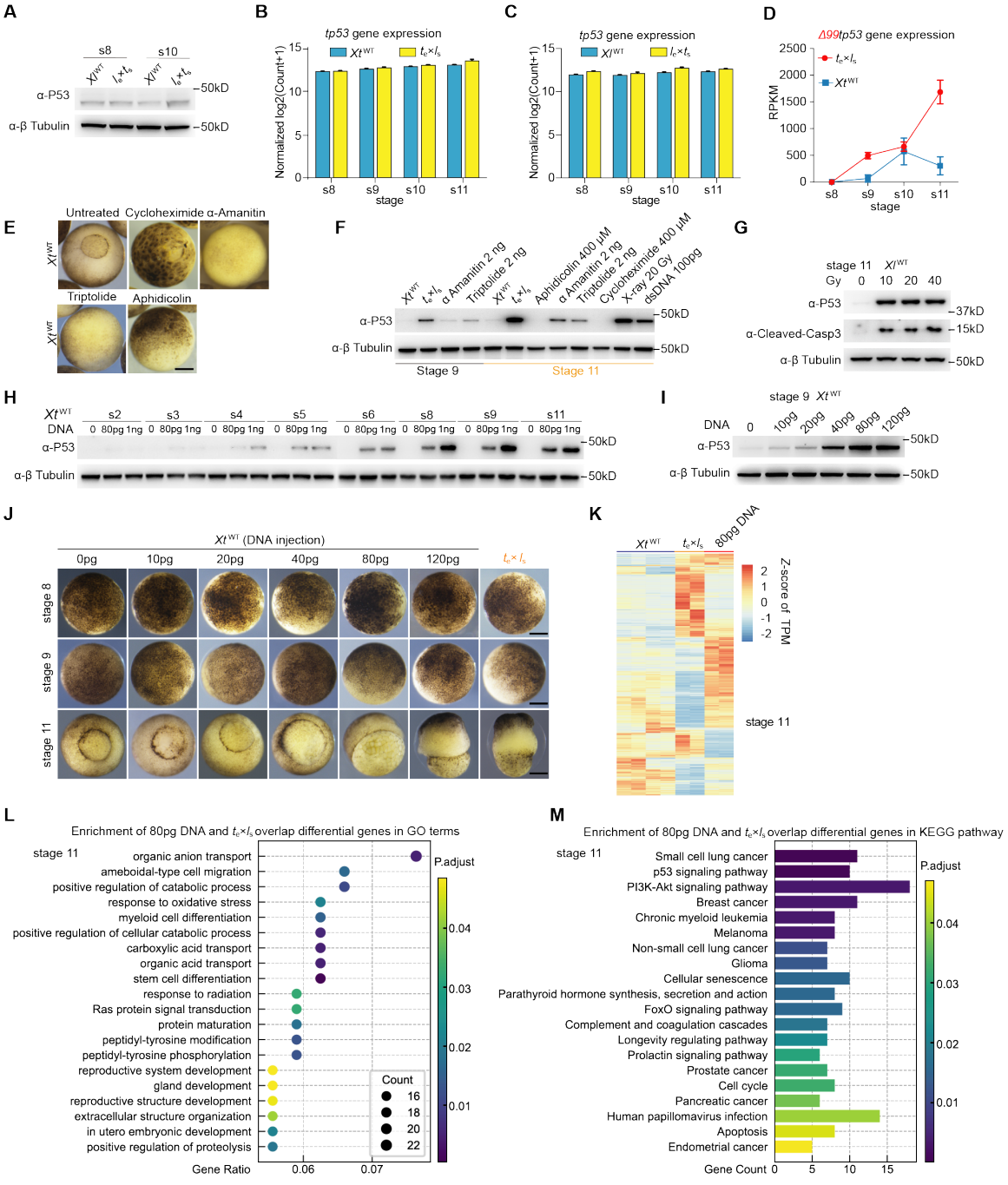

Figure S2. Robust P53 stabilization was induced in l_s×t_s hybrids, X-ray-irradiated embryos, and linear plasmid DNA-injected embryos. (A) Western blot data show that no P53 stabilization was induced in l_s×t_s hybrids. Stable low levels of P53 protein could be detected in both *Xl*^{WT} and l_s×t_s stage 8 and 10 embryos. As expected, the full-length P53 of *X. laevis* is smaller than that of *X. tropicalis* (compared to F). s, stage; β Tubulin, loading control. Identical results were obtained in three independent experiments. **(B)** Relatively stable *tp53* RNA levels in *Xt*^{WT} and t_e×l_s embryos at 4 different developmental stages, as revealed by RNA-seq analysis. Error bars, SD. **(C)** Relatively stable *tp53* RNA levels in *Xl*^{WT} and l_s×t_s embryos at 4 different developmental stages, as revealed by RNA-seq analysis. Error bars, SD. **(D)** *Δ99tp53* RNA levels in *Xt*^{WT} and t_e×l_s embryos at 4 different developmental stages, as revealed by RNA-seq analysis. Error bars, SD. **(E)**

Representative images show the developmental arrests of *Xt*^{WT} embryos induced by cycloheximide (400 μM), α-amanitin (2 ng), triptolide (2 ng), or aphidicolin (400 μM).Identical results were obtained in three independent experiments. Scale bar, 200 μm. **(F)** Western blot data show the detection of P53 stabilization in $t_e \times I_s$ hybrids, as well as in *Xt*^{WT} embryos subjected to various treatments as indicated. Identical results were obtained in three independent experiments. β Tubulin was used as a loading control. **(G)** Western blot data show induction of P53 stabilization and Caspase 3 activation in stage 11 wild-type *X. laevis* embryos upon X-ray irradiation at stage 6. Identical results were obtained in three independent experiments. β Tubulin was used as a loading control. **(H)** Western blot data show dose-dependent stabilization of P53 protein in *X. tropicalis* embryos upon injection of linear plasmid DNA. Identical results were obtained in three independent experiments. s, stage; β Tubulin, loading control. **(I)** Western blot data showing dose-dependent stabilization of P53 in *Xt*^{WT} embryos upon injection of linear plasmid DNA. Identical results were obtained in three independent experiments. β Tubulin, loading control. **(J)** Representative images showing gastrulation defects in *Xt*^{WT} embryos induced by exogenous DNA in a dose-dependent manner. Identical results were obtained in three independent experiments. Scale bars, 200 μm. **(K)** Heatmaps showing relative expression of all differential expression genes among the four groups of embryos at stage 11 (4,197 genes with $q < 0.05$ and absolute fold change > 2). **(L)** GO term enrichment analysis of stage 11 overlapping differential expression genes between the $t_e \times I_s$ group and the 80 pg DNA injection group. **(M)** KEGG pathway enrichment analysis of stage 11 overlapping differential expression genes between the $t_e \times I_s$ group and the 80 pg DNA injection group. Of note, P53 and FoxO pathways were identified.

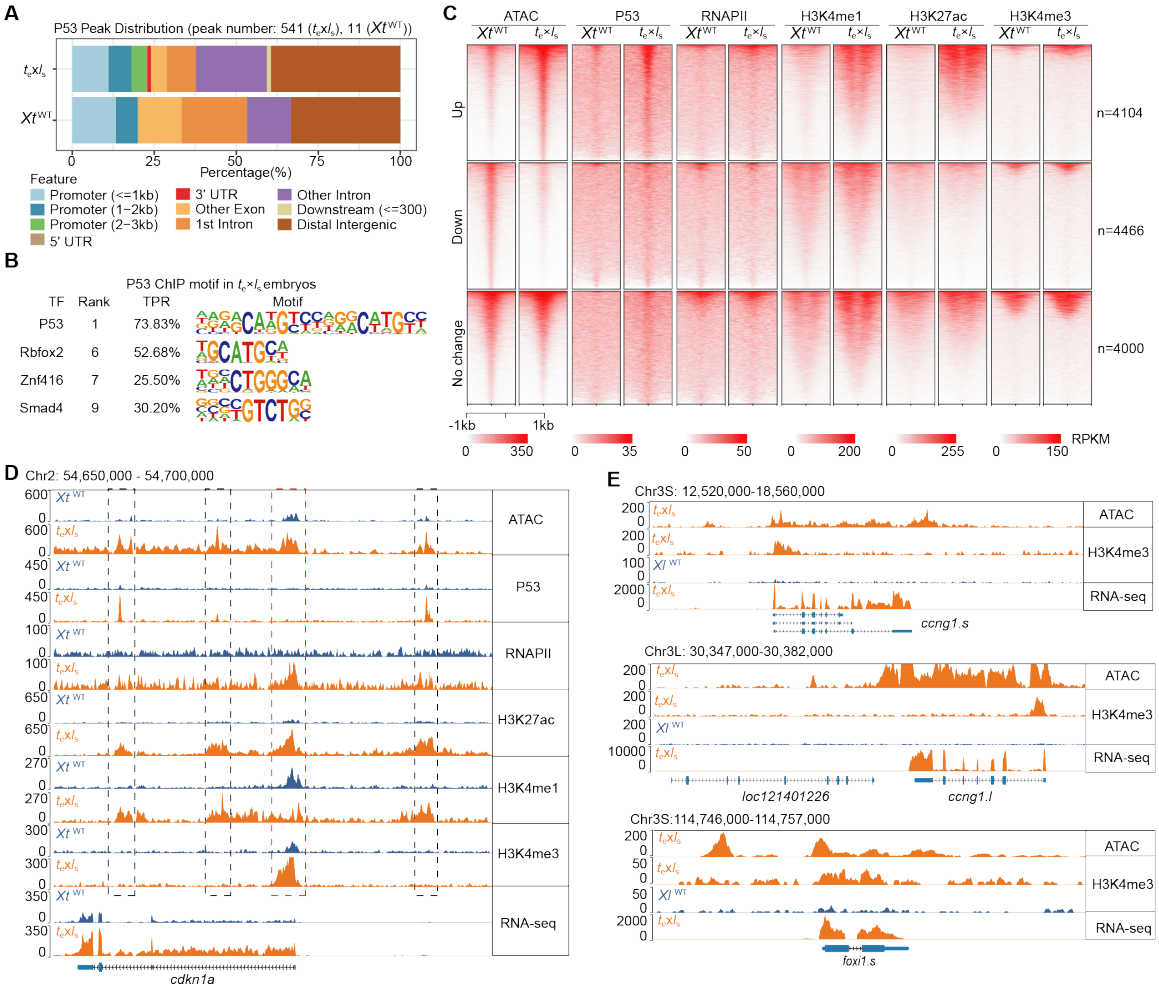

Figure S3. Activation of P53 signaling pathway in stage 9 t_e×l_s embryos. (A) Genomic distribution of P53 ChIP-seq signals from Xt^{WT} and t_e×l_s. **(B)** Motif enrichment of t_e×l_s P53 ChIP-seq peaks showing P53 itself as the most enriched one. **(C)** Heatmaps showing correlation of up-regulated ATAC-seq signals with increased P53, RNA Pol II, H3K4me1, H3K27ac, and H3K4me3 ChIP-seq signals in stage 9 t_e×l_s versus Xt^{WT}. Heatmaps were centered at open chromatin summits. Regions were ranked by the average open chromatin within 1 kb of the peak. The no change regions (4000) were randomly picked from all no change regions (50876). **(D)** Representative genome tracks showing transcriptional activation of P53 target gene *cdkn1a* (the *X. tropicalis* version) in t_e×l_s embryos at stage 9. **(E)** Representative genome tracks showing transcriptional activation of paternal (*X. laevis*) P53 target genes *ccng1.l*, *ccng1.s*, and *foxi1.s* (the *X. laevis* version) in t_e×l_s embryos at stage 9.

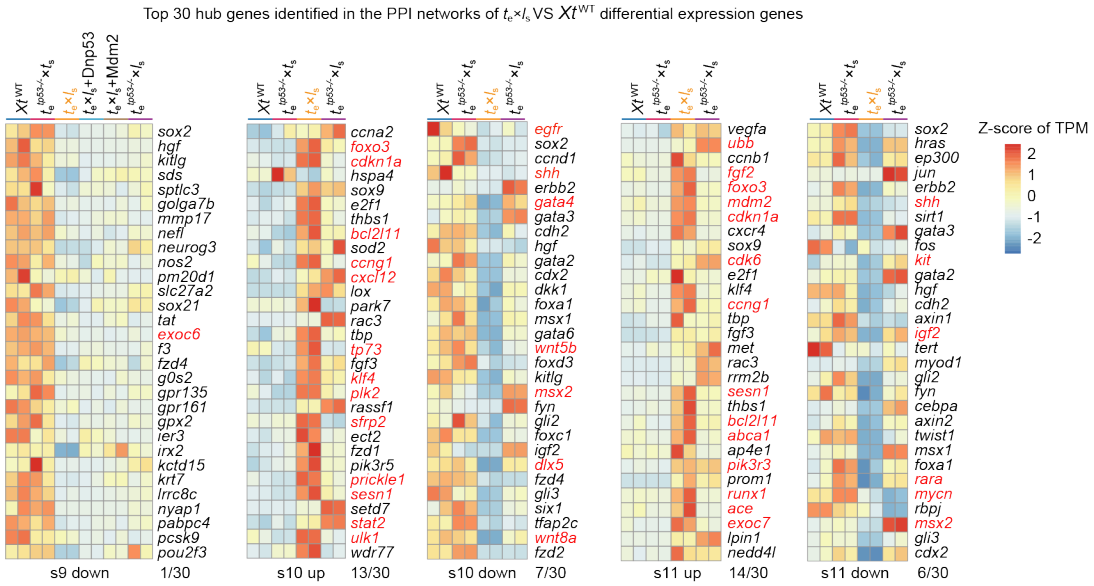

Figure S4. P53 regulates significant number of up-regulated top hub genes between $t_e \times l_s$ and Xt^{WT}. Heatmaps showing the top 30 hub genes identified in the PPI networks of differentially expressed genes between $t_e \times l_s$ and Xt^{WT} from stage 9 to stage 11. Genes in red were covered by corresponding P53 ChIP-seq signals.

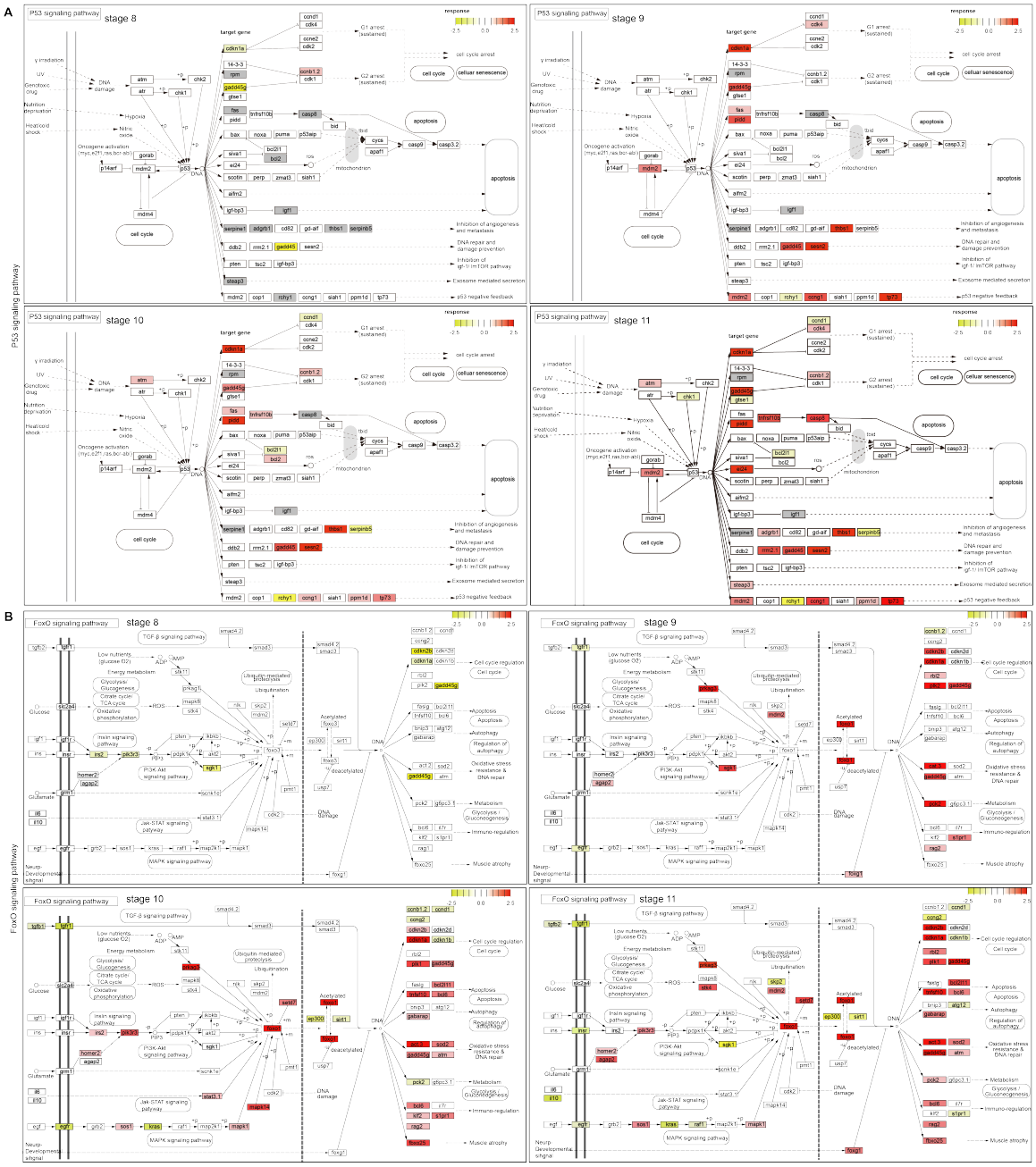

Figure S5. Dynamics of P53 and FoxO signaling pathway activities in $t_e \times I_s$ during stages 8-11. (A) P53 signaling pathway. **(B)** FoxO signaling pathway. Applying all the differentially expressed genes between $t_e \times I_s$ and Xt^{WT} from stage 8 to stage 11 to these two pathways revealed the activity dynamics of these two pathways during these developmental stages in $t_e \times I_s$. Up- and down-regulated genes were marked in red and yellow, respectively. These charts were generated on the KEGG PATHWAY Database and drawn by hand.

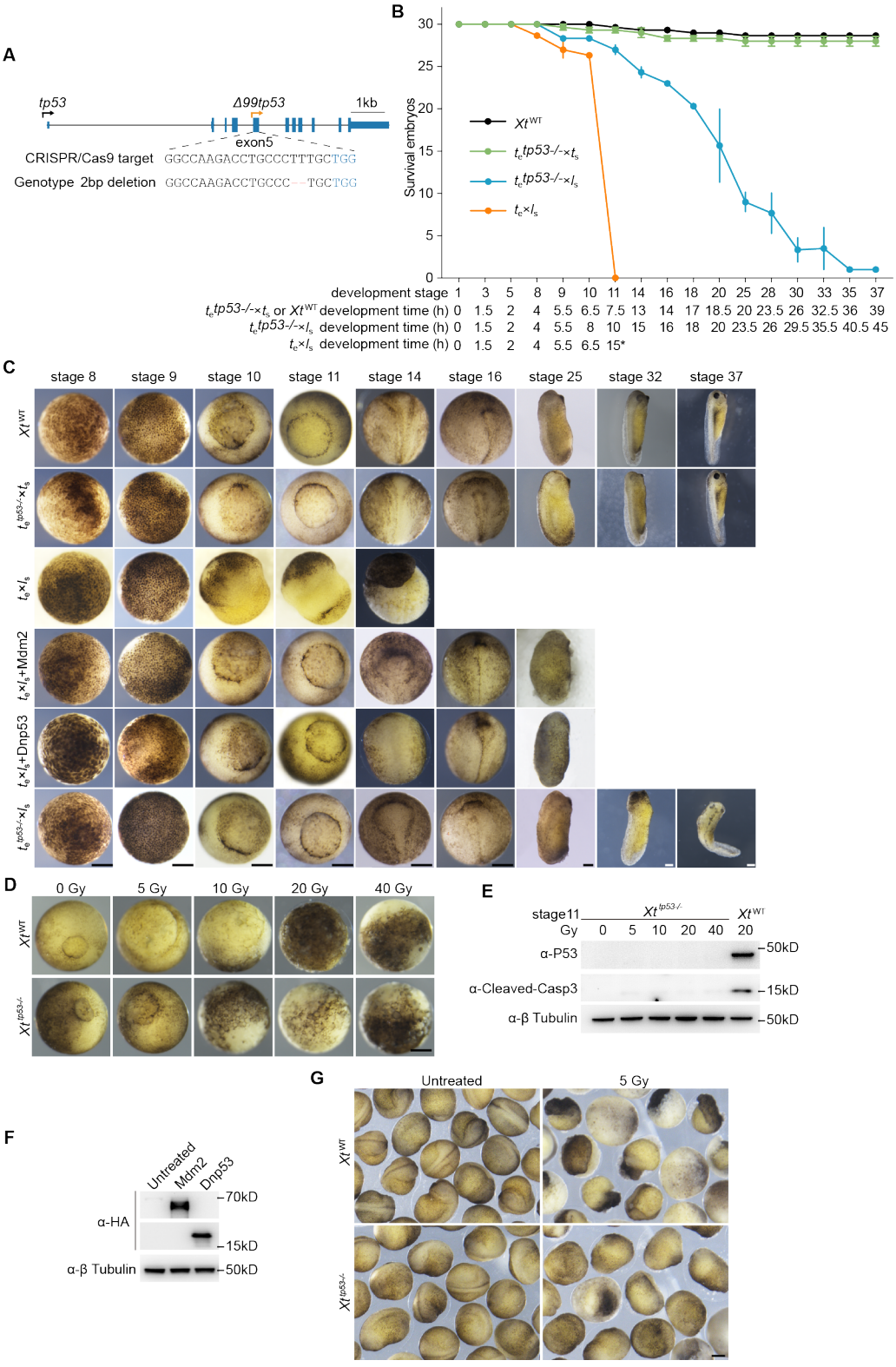

Figure S6. Inhibition of P53 activity rescued the early lethality of t_e×l_s hybrids, as well as the gastrulation defects of Xt^{WT} embryos induced by low doses of X-ray irradiation. (A) A schematic showing

CRISPR/Cas9-mediated *tp53* knockout strategy in *X. tropicalis*. **(B)** Statistics on the survival rates of indicted embryos from three independent experiments based on NF stages and developing time (h). Error bars, SD. **(C)** Representative images showing three ways of rescuing the lethality of $t_e \times l_s$. Identical results were obtained in three independent experiments. Scale bars, 200 μm. **(D)** Representative images of stage 12 embryos show that disruption of *tp53* can hardly rescue gastrulation defects induced by X-ray irradiation at doses above 5 Gy. Identical results were obtained in three independent experiments. Scale bar, 200 μm. **(E)** Western blot data of stage 11 embryos confirmed no P53 stabilization and revealed no caspase 3 activation in $Xt^{tp53-/-}$ embryos upon X-ray irradiation. Identical results were obtained in three independent experiments. β Tubulin was used as a loading control. **(F)** Western blot data of stage 9 embryos confirm expression of proper Mdm2 and Dnp53 proteins when the corresponding mRNAs were injected into $t_e \times l_s$ hybrid embryos. β Tubulin was used as a loading control. **(G)** Representative images show that disruption of *tp53* was able to rescue the gastrulation defect in *X. tropicalis* induced by 5 Gy of X-ray, allowing for the formation of normal neurulae. Identical results were obtained in three independent experiments. Scale bar, 200 μm.

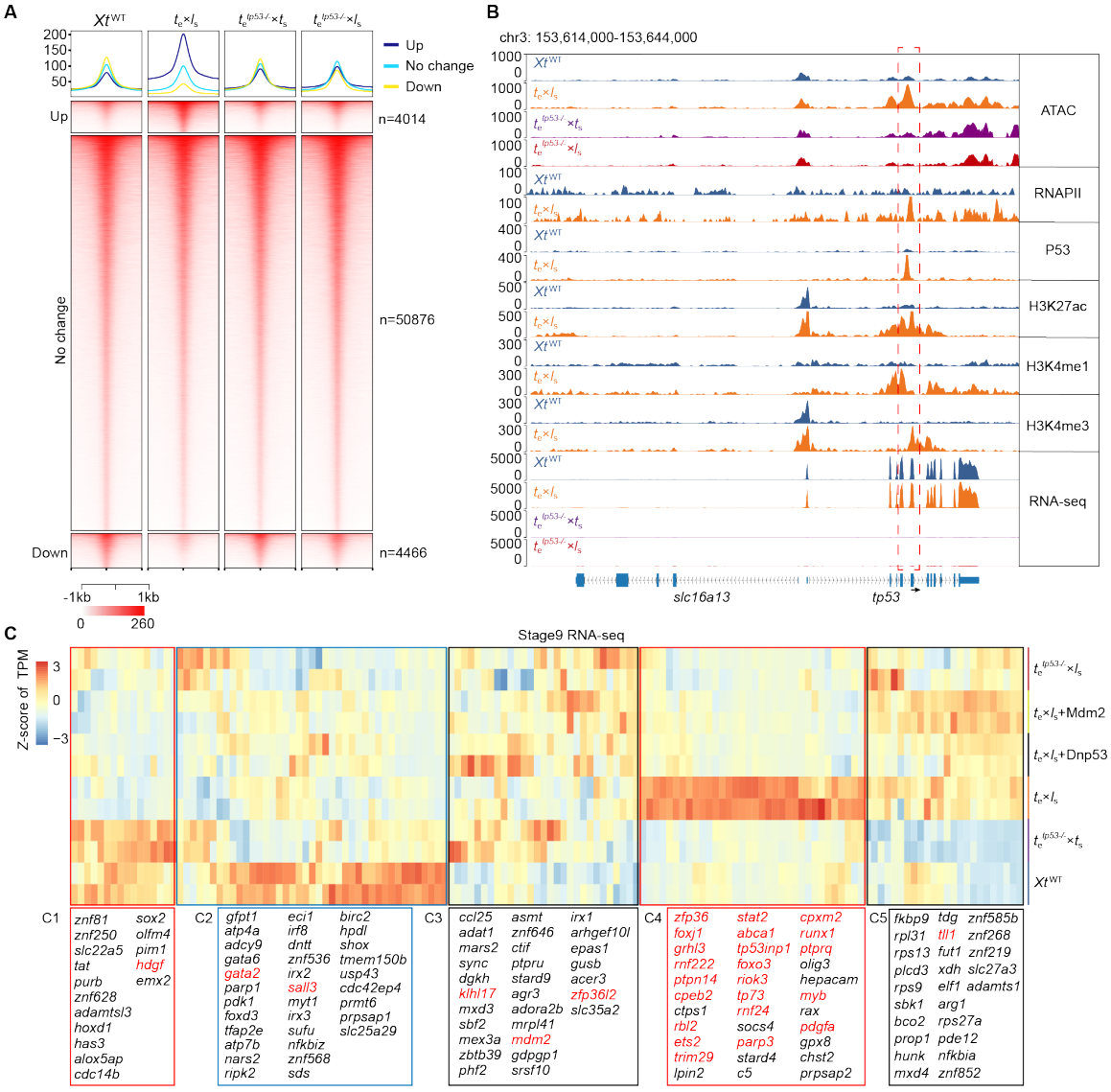

Figure S7. Molecular evidence of rescuing $t_e \times l_s$ lethality via inhibition of P53 activity. (A) Heatmaps showing rescue of the up- and down-regulated ATAC-seq peaks between stage 9 $t_e \times l_s$ and Xt^{WT} via knockout of maternal *tp53* gene ($t_e^{tp53-/-} \times l_s$). **(B)** Representative *X. tropicalis* genome tracks show the activation of *Δ99tp53* transcription in stage 9 $t_e \times l_s$ embryos, which was rescued by depletion of maternal P53. The red dashed box highlights the internal promoter region for *X. tropicalis Δ99tp53* transcription. **(C)** Heatmaps showing the relative expression of the 165 previously reported metabolism genes[2] in stage 9 embryos as indicated. Genes in red were covered by corresponding P53 ChIP-seq signals.

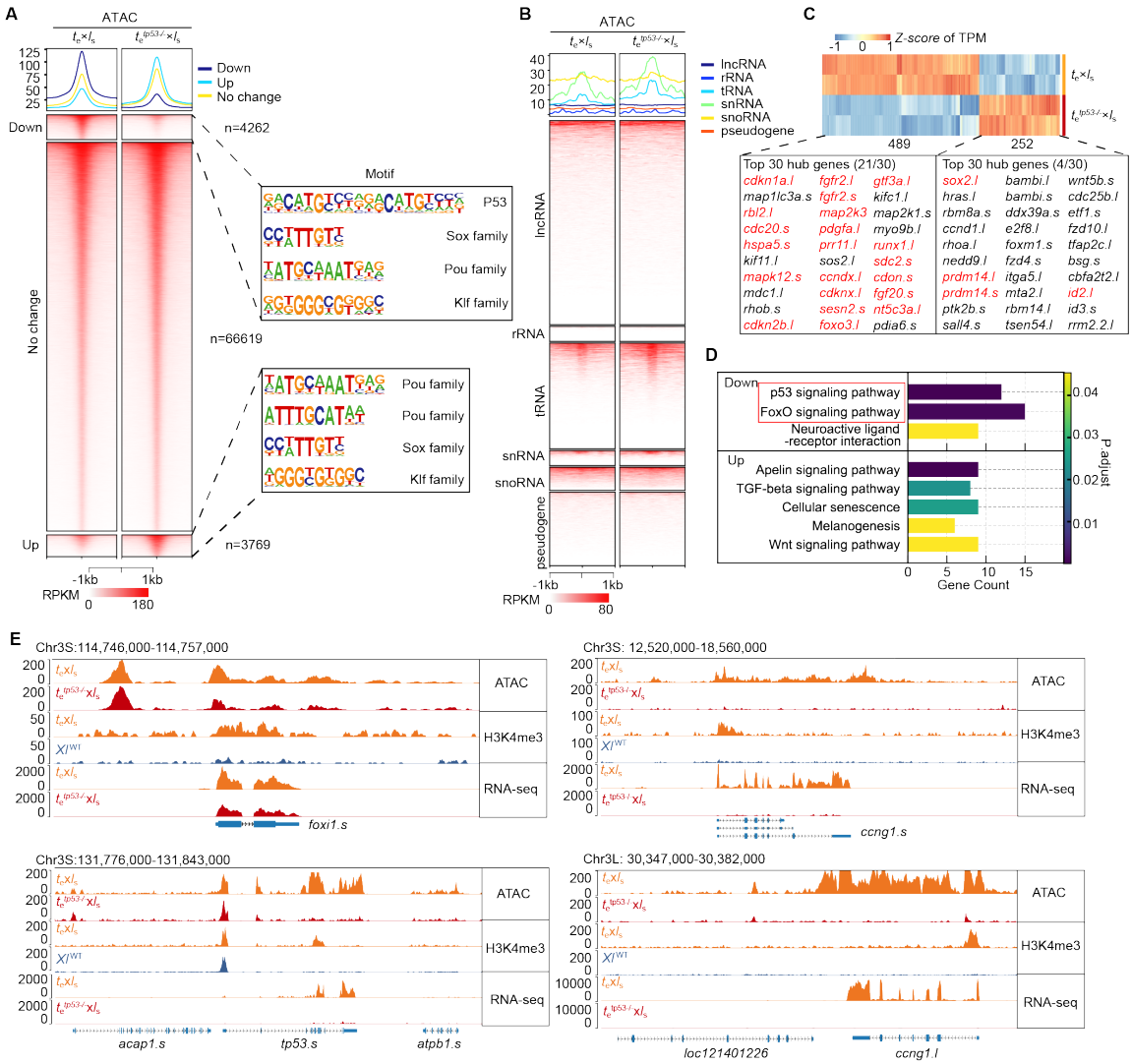

Figure S8. P53 pathway as the top one identified by comparative analysis of paternal genome-specific data between $t_e \times I_s$ and $t_e^{tp53-/-} \times I_s$. (A) ATAC-seq heatmaps based on *X. laevis* genome and the enriched motifs showing P53 binding motif as the most enriched one in the down-regulated peaks between $t_e \times I_s$ and $t_e^{tp53-/-} \times I_s$ at stage 9. **(B)** Heatmaps showing the distribution of ATAC-seq signals in different noncoding RNA gene loci and pseudogene in *X. laevis* genome. **(C)** Heatmaps showing relative expression of differential expression genes from paternal (*X. laevis*) genome between $t_e \times I_s$ and $t_e^{tp53-/-} \times I_s$ embryos at stage 9 (741 genes with $q < 0.05$ and absolute fold change > 2). Top 30 up- and down-regulated hub genes were identified by PPI analysis. Genes in red were covered by P53 ChIP-seq sginals. **(D)** KEGG pathway enrichment analysis of differentially regulated genes from *X. laevis* genome between $t_e \times I_s$ and $t_e^{tp53-/-} \times I_s$ embryos at stage 9 identifies P53 and FoxO pathways (red box) as the top down-regulated ones. **(E)** Representative *X. laevis* genome tracks showing rescue of activated P53 target gene transcription upon depletion of maternal P53.

Table S1. Sequences of primers for the cloning of four *X. tropicalis* genes and amplification of the pBluescript II SK+ plasmid

X. tropicalis dnp53 (*X. tropicalis tp53* NCBI Nucleotide accession no. NM_001001903.1)	*xt.tp53*-F：cggatagaaacagagcgaccg
	xt.tp53-R：gagcccccaaacacataatga
	pCS-*dnp53*-F1： ttcgaattcaaggcctatggaaccttcttctgagaccggcatgtccagtgaccctccac
	pCS-*dnp53*-R1： gtggagggtcactggacatgccggtctcagaagaaggttccataggccttgaattcgaa
	pCS-*dnp53*-F2：tcttctgagaccggcatgtccagtgaccctccacttccc
	pCS-*dnp53*-R2：actcactatagttctagatcactcggagtcctgcagctc
	xt.dnp53-4×HA-F： acttgttctttttgcaggatcccatcgatatggaaccttcttctgagaccggc
	xt.dnp53-4×HA-R： tatggatagccgggccccatggttctagactcggagtcctgcagctcatc
X. tropicalis mdm2 (NCBI Nucleotide accession no. NM_001244760)	*xt.mdm2*-F：aagtaagataaaacggctggaaga
	xt.mdm2-R：tgccaaataaggtgtctaaagatc
	xt.mdm2-4×HA-F： acttgttctttttgcaggatcccatcgatatggcggagggagagggctgc
	xt.mdm2-4×HA-R： tatggatagccgggccccatggttctagagctaaagtatgttagcacgatc
X. tropicalis bcl2 (NCBI Nucleotide accession no. XM_002934396)	*xt.bcl2*-F:gctgtttgagtagttctgggcg
	xt.bcl2-R:taaattgtcggatggtgaggct
X. tropicalis xiap (NCBI Nucleotide accession no. XM_031890487)	*xt. xiap*-F:ttgtgaaatagggcttgttacatg
	xt. xiap-R:gaagcagccatactgtttgtctag
dsDNA amplification	pBS-F：actcactatagggcgaattgggtac
	pBS-R：ctcactaaagggaacaaaagctgg